

# Indoor Environment Data Time-Series Reconstruction Using Autoencoder Neural Networks

Antonio Liguori<sup>\*,a</sup>, Romana Markovic<sup>b</sup>, Thi Thu Ha Dam<sup>a</sup>, Jérôme Frisch<sup>a</sup>, Christoph van Treeck<sup>a</sup>, Francesco Causone<sup>c</sup>

<sup>a</sup>E3D - Institute of Energy Efficiency and Sustainable Building, RWTH Aachen University, Mathieustr. 30, 52074 Aachen, Germany

<sup>b</sup>Building Science Group, Karlsruhe Institute of Technology, Englerstr. 7, 76131 Karlsruhe, Germany

<sup>c</sup>Department of Energy, Politecnico di Milano, Via Lambruschini 4, 20156 Milano, Italy

---

## Abstract

As the number of installed meters in buildings increases, there is a growing number of data time-series that could be used to develop data-driven models to support and optimize building operation. However, building data sets are often characterized by errors and missing values, which are considered, by the recent research, among the main limiting factors on the performance of the proposed models. Motivated by the need to address the problem of missing data in building operation, this work presents a data-driven approach to fill these gaps. In this study, three different autoencoder neural networks are trained to reconstruct missing indoor environment data time-series in a data set collected in an office building in Aachen, Germany. The models are applicable for different time-series obtained from room automation, such as indoor air temperature, relative humidity and  $CO_2$  data streams. The results prove that the proposed methods outperform classic numerical approaches and they result in reconstructing the corresponding variables with average RMSEs of 0.42 C, 1.30 % and 78.41 ppm, respectively.

**Keywords:** indoor environment data time-series, machine learning, data analytics, autoencoder, neural networks.

---

---

\*Corresponding author. Tel.: +49 241 80 25541;  
E-Mail: liguori@e3d.rwth-aachen.de

## 1. Introduction

In the European Union buildings account for more than 40 % of the total final energy consumption and approximately 36 % of  $CO_2$  emissions [1]. As a consequence, reliable estimation of building consumption data could foster energy efficiency strategies, such as the analyses of retrofit options [2] or the development of fault detection and diagnosis (FDD) schemes [3]. In the related research, two approaches are generally followed to achieve this goal [4]: forward modeling and data-driven modeling. While the former is based on solid engineering principles, the latter relies on data collected during normal or predetermined system operation and it can usually capture more accurate as-built system's performance with a limited number of known parameters [4]. Additionally, data-driven approaches can be successfully applied to represent energy-related human actions in buildings (e.g. window openings), being the result of a number of stochastic driving forces [5, 6].

By definition, data-driven modeling explicitly requires the availability of useful data [7]. Therefore, missing values present the major limitation on this approach [8–10]. As stated by multiple studies [7, 8], data gaps are a common problem in building automation systems (BAS) and they may be caused by a number of reasons such as power outages, sensors defects, communication problems or network issues. As a result, the presence of these anomalies could significantly reduce the size of the available data set and hinder further energy analysis [11, 12]. So far, existing studies have handled missing data either using simplified methods [8] or excluding them from further analytics due to the lack of ground truth values [7]. In summary, both latter approaches have usually led to limited inserting accuracy and lower resulting model performance [7, 8].

The aim of this paper is to propose a method for reconstructing missing sequences of indoor environment data obtained from room control sensors. For that purpose, a data set collected in an office building in Aachen, Germany, was analyzed and preprocessed. Models for handling missing data points were implemented, trained and evaluated on indoor air temperature ( $T$ ), relative humidity ( $RH$ ) and  $CO_2$  concentration data. In particular, three promising autoencoder architectures were investigated: feed-forward denoising autoencoder, convolutional denoising autoencoder and long short-term memory (LSTM) denoising autoencoder. Eventually, the performance of the proposed methods were compared to analytical methods based on polynomial interpolations.

Even though the related research has already identified autoencoders as a promising technique to address missing values and anomalies in monitoring building data sets [13–16], some significant research questions are still unaddressed. In particular, the existing studies have often focused on reconstructing a single type of signal or they have been limited by the small amount of available training data and computational power. Motivated by the latter open, yet significant research question, this work presents an autoencoder-based method for reconstructing and forecasting indoor environment data time-series. The models were developed using monitoring data from more than 70 offices over four years, which resulted in almost 100,000 monitoring days. Eventually, the optimal problem hypothesis was identified based on the results obtained from 7,000 core hours of GPU and CPU computations.

Additionally, the scientific contribution of the presented work consists of the following:

- To analyze the variability of univariate artificial neural networks (ANNs) performance when applied to different kinds of indoor environment data time-series.
- To present a generalized gap-filling method to address the problem of missing values in building data sets.
- To propose a solution to address the issue of ANNs' saturation for energy systems applications.

The rest of this paper is organized as follows: Section 2 presents the motivation that led to the development of a missing data inserting model based on autoencoder neural networks. Section 3 provides the reader with further information on the used data set and on the models' theory and implementation. Section 4 presents results on developing a suitable tool for indoor environment data time-series reconstruction. Finally, the results and novel findings are discussed and summarized in Sections 5 and 6.

Table 1: List of abbreviations.

ANNs	artificial neural networks
BAS	building automation systems
BIT	bi-directional imputation and transfer learning
CR	corruption rate
DBN	deep belief network
ELM	extreme learning machine
FDD	fault detection and diagnosis
FFT	fast fourier transform
GANs	generative adversarial networks
IAQ	indoor air quality
IQR	interquartile range
LSTM	long short-term memory
MAE	mean absolute error
MELs	miscellaneous electric loads
MSE	mean squared error
NRMSE	normalized root mean squared error
OB	occupant behavior
RBM	restricted boltzmann machines
RF	random forest
RH	indoor relative humidity
RMSE	root mean squared error
SAT	saturation performance metric
SGD	stochastic gradient descent
T	indoor air temperature

## 2. Background

### 2.1. Missing data in buildings' control

The importance of sufficient large data sets on time-series modeling was empirically explored in the scope of the Texas LoanSTAR program [11], whose objective was to measure savings from energy conservation retrofits. By increasing the length of building data sets from one to five months, the average cooling prediction error decreased from 7.3 % to 3.0 % and the annual heating prediction error decreased from 27.5 % to 12.9 %. Zapata et al. [12] discovered also that a fast fourier transform (FFT), as applied to assess the frequency content of time-series wind speed data, gave unacceptable results when information loss was at least 2.5 % of the data set.

As pointed out by Chong et al. [8], in 2016 there was still little relevant research about handling missing values in building data sets. As a consequence, existing studies often relied on simplified methods such as complete case analysis, mean inserting and zeros inserting [8]. However, these methods often resulted in poor reconstruction of missing data, which could lead to limited performance of later applied data-driven models. In a recent study, Candanedo et al. [9] reconstructed the average indoor air temperatures of a passive house, achieving accurate results with a random forest (RF) model. However, the proposed model used as input features multiple time-series (e.g. external weather data, total electrical energy use) that could not be always known for a data reconstruction problem. Furthermore, when the same outputs were used to reconstruct the single-room air temperature, the performance of the proposed method dropped significantly. The use of more advanced deep learning techniques for the reconstruction of building energy data was explored by Ma et al. [10]. By applying a LSTM with bi-directional imputation and transfer learning (BIT), the same author managed to achieve a reconstruction error approximately 30 % less than linear interpolation models, in case of continuous missing electrical power data. Conclusively, Benitez et al. [13] coupled multivariate variational autoencoders with convolutional layers to estimate missing indoor air quality (IAQ) subway data. The results proved that a correct reconstruction of IAQ data gaps could have a direct impact on the subway ventilation system's performance. However, a strong limitation of this study was the size of the used data set, namely 1 month of measurements with hourly resolution.

## 2.2. Deep learning methods for buildings' control

Given the recent findings in the related literature [10, 13–16], the modeling methods adopted in this study belong to the category of deep learning.

Deep learning models are neural networks with learned feature representation over multiple hidden layers [17]. In the related building research, these methods have been extensively used for energy consumption and occupant behavior (OB) modeling applications [5, 18–37]. Qian et al. [23] explored the potential of ANNs for HVAC load forecasting, when applied to small amount of data. The results proved that the fitting degree of the proposed models was over 85 %. They pointed out the importance of the sufficiently large training data set. In particular, the use of a smaller training set that consisted of one month and one week of monitoring data led to accuracy decrease for 6 % and 20 %, respectively. Zhang et al. [25] trained a deep belief network (DBN) and extreme learning machine (ELM) based framework to predict half-hourly building energy consumption data. Here, DBNs consisted of a stack of restricted boltzmann machines (RBMs), where RBMs had fully connected visible and hidden layers [25]. The correspondent mean absolute error (MAE) was 10 % higher than the results obtained by support vector regression. Yan et al. [30] addressed the issue of the imbalanced properties of training data sets for automatic FDD of chillers. They used generative adversarial networks (GANs) to generate faulty training samples. The results proved that without the implemented model, classification accuracy could hardly reach 90 %. Conclusively, Markovic et al. [37] developed a LSTM neural network for day-ahead prediction of miscellaneous electric loads (MELs). The proposed implementation outperformed benchmark approaches based on Weibull distribution and Gaussian mixture methods when MELs and occupancy information data were used as input parameters to the model.

## 2.3. Autoencoder neural networks for buildings' control

Autoencoders are ANNs which learn to reconstruct original inputs from a noisy version, making missing data reconstruction one of their reasonable applications [38]. However, few studies applied these models in the field of building energy systems [39], further emphasizing the relevance of this work. In this regard, Fan et al. [14] explored the potential of different types of autoencoder neural networks in the anomaly detection of building operational data. The results showed that a 1D convolutional architecture could effectively capture the intrinsic characteristics in building energy data, while preserving the temporal data information. Liu et al. [15] applied different machine learning-based anomaly detection methods to vertical plant wall systems. The results confirmed that the autoencoder configuration outperformed other models for both contextual and point anomaly detection of temperature and  $CO_2$  data. Finally, Araya et al. [16] used autoencoders to capture HVAC consumption patterns and they used the gained knowledge to identify abnormal consumption behaviours in the same system.

## 3. Methodology

The aim of this paper is to develop an approach for filling indoor environment data gaps. For that purpose, three different autoencoder neural network architectures were implemented in order to identify the optimal model hypothesis. In this respect, room temperature, relative humidity and  $CO_2$  concentration data were artificially corrupted, by setting to zero sub-daily sequences of random length. In particular, the reconstructed gaps ranged between few hours (10 % of the daily values) and around 22 hours (90 % of the daily values). A summary of the adopted modeling approach is proposed in Figure 1.

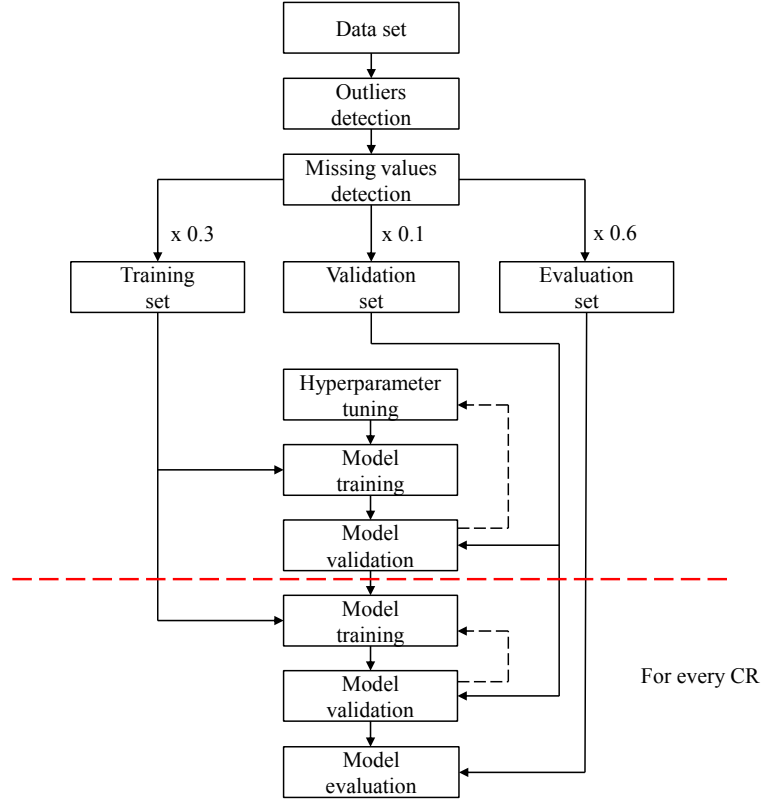


Figure 1: Modeling flowchart. CR is the applied masking noise.

### 3.1. Denoising autoencoder neural networks

The general structure of an autoencoder is presented in Figure 2. An autoencoder neural network is a representation learning approach which turns incoming data into different representations, through an encoder function, and reconstructs the original input through a decoder function [17].

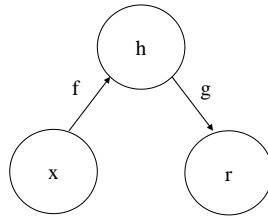


Figure 2: Working principle of a general autoencoder. Figure reproduced based on Goodfellow [17].

Input  $x$  is mapped to an output reconstruction  $r$  through an internal representation  $h$ , namely code. The autoencoder has two components: the encoder  $f$  (mapping  $x$  to  $h$ ) and the decoder  $g$  (mapping  $h$  to  $r$ ) [17].

The encoder is defined as [17]:

$$h = c(Wx + b), \quad (1)$$

while the decoder is formulated as:

$$r = c(W'h + b'), \quad (2)$$

where  $c$  is a non-linear function, called activation function,  $W$  and  $W'$  are called weights,  $b$  and  $b'$  are called biases. By implementing activation several times (training), the model could acquire useful knowledge about the systems' properties [17].

The structure of a denoising autoencoder is presented in Figure 3, while its extension to the stacked denoising autoencoder is presented in Figure 4. In contrast to a general autoencoder, a denoising autoencoder receives a corrupted input  $x^*$  and is trained to reconstruct the original uncorrupted data  $x$  [17].

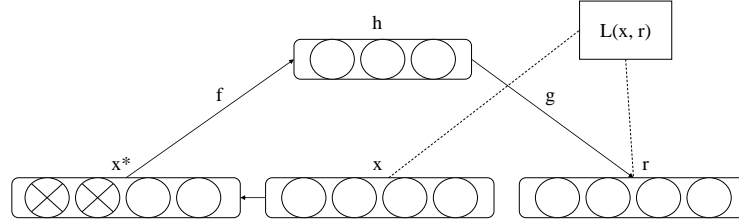


Figure 3: Working principle of a denoising autoencoder. Figure reproduced based on Vincent et al. [40].

The training process consists of minimizing a loss function  $L(x, r)$  which quantifies the difference between the original input and output at each step. In this study, corruption of input data is performed by setting to zero an interval of sequential values of random length. This approach is used to simulate how missing data are distributed.

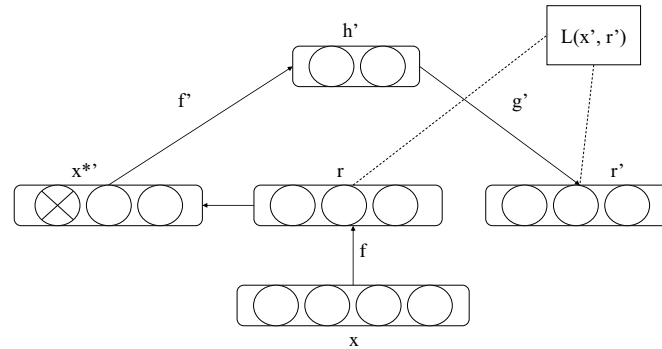


Figure 4: Working principle of a stacked denoising autoencoder. Figure reproduced based on Vincent et al. [40].

After the first level of denoising autoencoder has been trained (Figure 3), a second level of denoising autoencoder is trained using the previously optimized encoding function,  $f$ . Corruption takes place on the output of the previous optimized layer  $r$  [40].

### 3.2. Data set

The used data were collected in the E.ON ERC main building, located in Aachen, Germany. The building under investigation has a usable area of  $7,500 \text{ m}^2$  over four storeys and it includes offices, seminar rooms, laboratories and common area [41–44].

Based on the logging frequency and monitoring duration, it could be expected that around 181 million sets of observations were collected for each variable from 2014 to 2017. The monitoring data were grouped in two subsets, namely data set "A" (2014-2015) and "B" (2016-2017). Data set "A" contained measurements for 73 rooms from 2014 and 2015, stored into "HDF5" data containers [45] on a monthly basis. Monitoring data for the years 2016 and 2017 were collected in 84 offices and they were stored in "pickle" files [46]. Here, each file contained data for a single office over the whole observed biannual period.

### 3.3. Data preprocessing

Before further analysis and modeling, data were cleaned and preprocessed. This step involved the detection of frequently encountered anomalies, such as missing values and outliers [47]. Missing values reduce the size of the available data set, hence compromising the reliability of the model's outcome [47]. Outliers are noisy data points with values significantly different from the majority of other data points [47]. For this reason, they could lead to underestimated or overestimated results [47]. For the detailed explanation of the adopted data cleaning procedure the reader is referred to the Appendix.

According to the existing literature [48–50], additional preprocessing, such as resampling resolution and data normalization was performed in order to increase performance and computational efficiency of the proposed models. Here, resampling resolution is the process of changing the frequency of time-series data [49], while data normalization is applied to prepare raw data for a better network use [50]. In particular, data were downsampled to 30 minutes frequency and normalized using the Statistical or Z-Score Normalization function [50]:

$$z = (x - u) / s, \quad (3)$$

where,  $x$  are data to normalize,  $u$  is the mean of the training samples and  $s$  is the standard deviation of the training samples. Before normalizing, data were split into training (30 %), validation (10 %) and test set (60 %) for every variable. In order to favour models generalization, limits were defined based on training set and eventually adopted for each of the three parts identically.

### 3.4. Model development

The models were developed using the Python programming language and open source libraries Tensorflow [51] and Keras [52]. Figure 5 shows the autoencoder structure as implemented in the scope of the performed experiments. The explored models included the architectures with one and up to three hidden layers per each encoder and decoder. Batch-normalization was included after every layer in order to avoid the network saturation for both feed-forward and convolutional autoencoders [53].

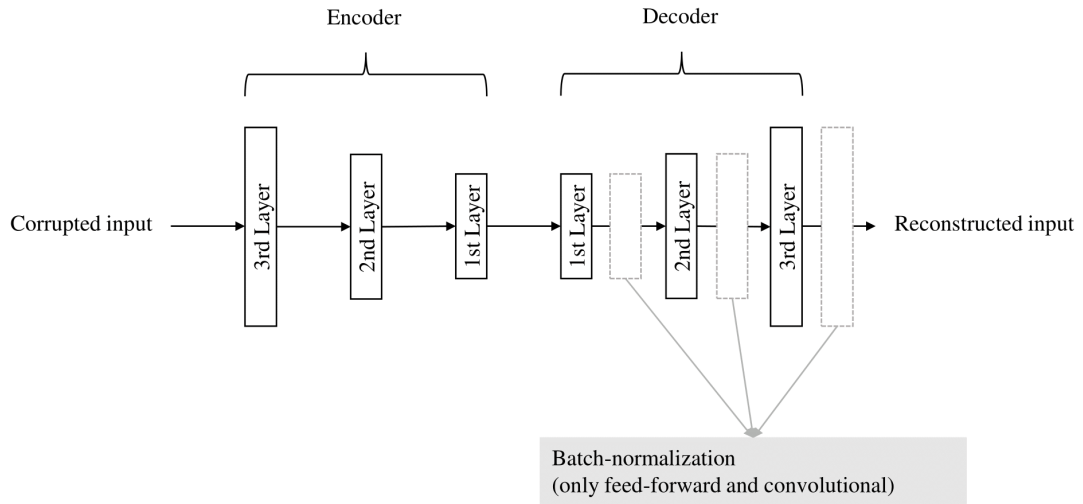


Figure 5: General autoencoder architecture with 3 layers per side.

Feed-forward denoising autoencoders were fed with unrolled half-hourly daily observations, which resulted in 48 features. Unrolling the 1-D temporal sequences into a single input layer is, indeed, a commonly adopted approach

to address temporal dependencies for a feed-forward neural network [5, 36]. However, feed-forward neural networks with unrolled sequences have separate parameters for each feature, which means that weights cannot be shared along the input series [17]. While convolutional neural networks apply the same kernel to every time-step, in the LSTM configuration each output node is a function of the previous one and parameters can be shared along very long sequences [17].

Models' overfitting was prevented by using an early stopping criteria based on the validation loss [17]. Furthermore, the mean squared error (MSE) loss function was applied to the reconstructed and original input over all the training samples, as follows [17]:

$$MSE = \frac{\sum_i^m (Y' - Y)_i^2}{m}, \quad (4)$$

where  $m$  is the batch size. In order to find the optimal parameters for the models, the MSE was minimized using either a stochastic gradient descent (SGD) optimizer with momentum [54] or Adam optimizer [55]. The optimizer choice was handled as an additional hyperparameter. In this study, the hyperparameter tuning was conducted separately for each target variable (temperature, relative humidity,  $CO_2$  concentration). Additionally, the whole hyperparameter range was explored for all neural units, such as feed-forward, LSTM and convolutional. The range of values in which the optimal model's configuration was investigated is summarized in Table 2.

Table 2: Overview of tuned hyperparameter and explored values.

Hyperparameter	Values
Hidden layers per side	1 - 3
Hidden layer units/ filters (convolutional)	8, 16, 32, 64, 128
Kernel size (convolutional)	2, 3, 5, 7, 11
Batch size	128
Learning rate	0.001, 0.01, 0.1
Optimizer	SGD with 0.9 momentum, Adam

It was opted for the grid search tuning over more advanced methods due to the relatively small researched hyperparameter space. Other tuning strategies, such as random or greedy search [56], would have been beneficial in case of more complex scenarios.

For every possible combination of hyperparameter, the score given to the model was obtained by averaging the MSEs, computed on the normalized validation set, with a corruption rate (CR) ranging between 0.2 and 0.8. Given the computational cost of this process, multiple independent jobs with different hyperparameters were run in parallel using the computational resources at the RWTH Aachen University Compute Cluster. In order to address the stochastic initialization of models' weights, the tuned configurations were run again 10 times and evaluated on the same validation data as before. Models with the lowest MSE were eventually exported for further evaluation on the test set.

## 4. Results

### 4.1. Performance evaluation metrics

The performance of missing data insertion was assessed using the root mean squared error (RMSE) method, since it is the established evaluation method by the existing research [9, 10, 13]. In order to obtain objective evaluation results, the RMSE was applied only to the corrupted sequence of the test data. Additionally, the ability of the proposed models for capturing indoor environmental data patterns was estimated by computing the RMSE on each sequence [14]. The RMSE equation is given as follows [9, 10, 14]:

$$RMSE = \sqrt{\frac{\sum_{i=1}^n (X_i^{obs} - X_i^{inserted})^2}{n}}, \quad (5)$$

where  $X_i^{obs}$  are the  $i$ -th real values,  $X_i^{inserted}$  are the  $i$ -th reconstructed values and  $n$  are the total number of data points on which RMSE is computed.



Comparison between different variables and studies was made by means of the normalized root mean squared error (NRMSE), obtained by normalizing the RMSE over the interquartile range (IQR), due to the possible presence of noisy data points:

$$NRMSE = \frac{RMSE}{IQR} . \quad (6)$$

#### 4.2. General observations during model development

Network saturation was identified to be a major modeling complexity in case of both feed-forward and convolutional denoising autoencoders. Formally, neural network saturation could be described as an impediment to gradient propagation [37, 57]. Its main effect was to produce always the same output, no matter how different the input sequence was.

As presented earlier, neural networks are trained by minimizing a loss function between targets and true values. This can be accomplished by applying an iterative algorithm called gradient descent [58]. The working principle of a gradient descent algorithm is simple: weights and biases are initialized to some values and then they are continuously updated in the direction that decreases the loss function, namely opposite to the gradient [58]. Each unit in a neural network receives signals and weights from previous units and computes a value called pre-activation [58]:

$$z = \sum_j w_j x_j + b , \quad (7)$$

where  $z$  is the pre-activation value,  $j$  is the number of input signals and weights,  $w$  are the weights,  $b$  is the bias which determines units' activation in case no inputs are present. The activation value is the pre-activation passed through an activation function  $\phi$  [58]:

$$a = \phi(z) . \quad (8)$$

If, during training, the activation of a neural network unit is always near the boundaries of its dynamic range (the possible outputs of an activation function), then the gradient of the pre-activation is very small and weights are not updated [58]. These neural network units are called saturated units [58]. Hence, saturated units can be identified looking at the histogram of the average activations and checking that they are not concentrated at the endpoints [58]. Different approaches are followed in the literature to avoid network saturation. Glorot and Bengio [57] proposed a novel normalized initialization for neural network weights:

$$W = U[-\frac{\sqrt{6}}{\sqrt{n_j + n_{j+1}}}, \frac{\sqrt{6}}{\sqrt{n_j + n_{j+1}}}] , \quad (9)$$

where  $W$  are the neural network weights,  $U$  is a uniform distribution function,  $n$  is the size of the  $j$ -th layer. Maas et al. [59] used ReLU activation functions as alternative to sigmoid and  $\tanh$ , causing in this way network saturation at exactly 0. Ioffe and Szegedy [53] proposed a new mechanism called batch-normalization, which ensures that distribution of nonlinearity inputs (i.e. pre-activations) remains more stable as the network trains.

In this study, since no other formal metrics were available at the current state of the research, network saturation was evaluated using the saturation performance metric (SAT) proposed by Markovic et al. [37], calculated over the normalized reconstructed values.

In order to guarantee an effective model training, all the previous approaches followed in the literature were implemented [53, 57, 59]. Figure 6 shows the histogram of the average activations for the original feed-forward denoising autoencoder configuration with classical uniform weights initialization, sigmoid activation functions and no batch-normalization. It is possible to observe the typical network saturation problem, being the average activations always concentrated at 0 and 1, namely the endpoints of a sigmoid activation function.

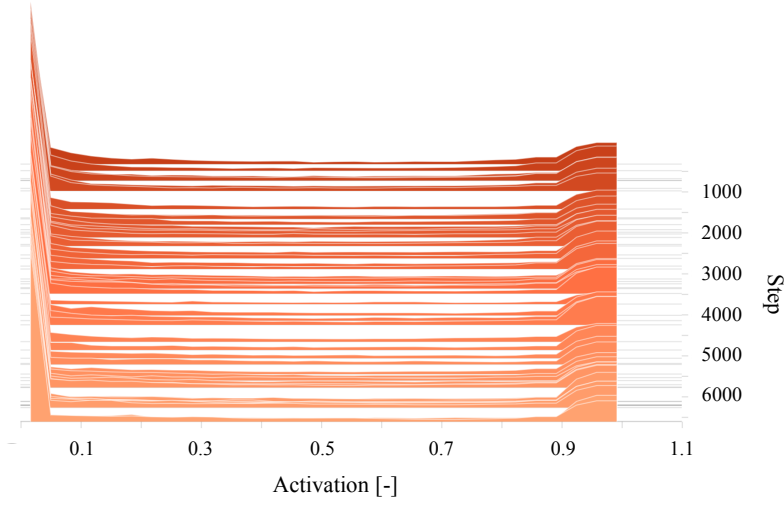


Figure 6: 3D Histogram of the average activations for the original feed-forward denoising autoencoder with 10 % corruption rate.

The use of normalized initialization, ReLU activation function and batch-normalization as proposed in the literature confirmed to reach higher performance and to overcome saturation problems. Figure 7 shows how average network activations change during training, not being stuck in any saturating point. Note that ReLU activation function was applied on the encoder layer while batch-normalization only in the decoder layer. The authors realized that higher performance could be reached using a *tanh* activation function in the decoder layer, in association with batch-normalization. Conclusively, the SAT results confirmed the superiority of the chosen models' configurations with respect to the original denoising autoencoder architectures with classical uniform weights initialization, sigmoid activation functions and no batch-normalization.

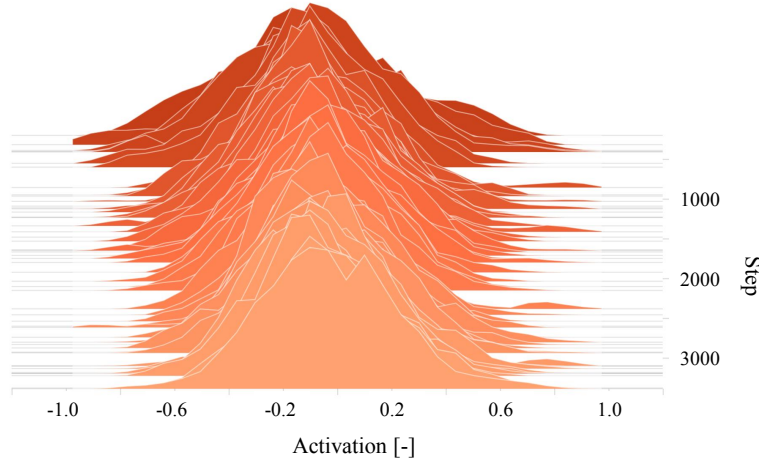


Figure 7: 3D Histogram of the average activations for the new feed-forward denoising autoencoder with 10 % corruption rate.

The saturation performance results of the proposed models for different CR are summarized in Table 3. Here, network saturation is defined as the SAT lower than 0.1 [37]. Every autoencoder was well above the previous defined limit, meaning that the adopted architecture strategies could efficiently overcome saturation issues. The above identified metric was function of the particular variable and of the applied CR. While the SAT was insensitive to changes in

CR for relative humidity, it decreased for both temperature and  $CO_2$  data.

Table 3: SAT for denoising autoencoder neural networks for different CR. "CONV", "FEED" and "LSTM" stand for convolutional, feed-forward and LSTM denoising autoencoder.

	CR [-]	$T$ [-]			$RH$ [-]			$CO_2$ [-]		
		CONV	FEED	LSTM	CONV	FEED	LSTM	CONV	FEED	LSTM
SAT	0.10	0.88	0.85	0.84	0.95	0.97	0.98	0.78	0.83	0.77
	0.20	0.87	0.83	0.79	0.95	0.98	0.98	0.71	0.77	0.76
	0.30	0.83	0.82	0.77	1.00	0.98	0.98	0.65	0.73	0.69
	0.40	0.77	0.75	0.73	0.99	0.96	0.99	0.75	0.66	0.59
	0.50	0.73	0.72	0.72	0.98	0.97	0.98	0.57	0.60	0.47
	0.60	0.73	0.68	0.65	0.97	0.95	0.95	0.52	0.46	0.35
	0.70	0.69	0.69	0.59	0.94	0.96	0.96	0.51	0.48	0.32
	0.80	0.64	0.64	0.60	0.92	0.94	0.94	0.44	0.41	0.30
	0.90	0.62	0.63	0.57	0.93	0.96	0.93	0.39	0.34	0.31
Average		0.75	0.73	0.70	0.96	0.96	0.97	0.59	0.59	0.51

#### 4.3. Data reconstruction performance evaluation

Firstly, the ability of autoencoder neural networks for capturing daily patterns of environmental data is assessed. Eventually, the proposed models' performance in reconstructing sub-daily indoor environment data gaps are evaluated and compared to classic polynomial interpolations.

Figure 8 shows the RMSE variance for a LSTM denoising autoencoder. In particular, the model was trained with a masking noise of 0.1 and applied to the non corrupted test sets. Here, the RMSE was computed on the single time-step as seen in Section 4.1. The average RMSEs over the number of test sequences were 0.027 C, 0.12 % and 4.25 ppm, respectively for  $T$ ,  $RH$  and  $CO_2$  data. Furthermore, all the reconstruction residuals computed with the LSTM architecture were lower than the convolutional and feed-forward ones.

Based on the boxplots presented in Figure 8, the observed days with RMSE out of the measured IQR are represented. These could be considered as sequences with atypical behavior, for which the indoor environment data patterns cannot be detected by the model. Figure 8 shows also, for every variable, how a random day with atypical behavior looks like and how it is reconstructed by the LSTM autoencoder. In particular, the represented sequence of relative humidity data presents an outlier in the early morning observation. This anomaly, which could be caused by sensors' malfunctioning, was not detected during the data preprocessing, but it was identified with the proposed model.

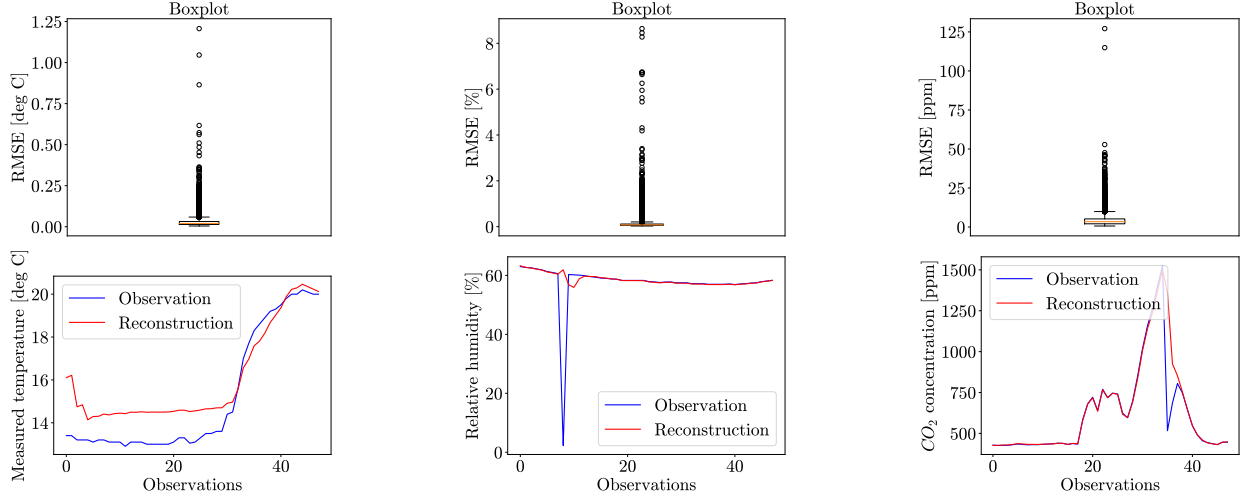


Figure 8: Boxplots of the observed sequences and reconstruction of a day with atypical behavior.

Table 4 summarizes the behavior of all the models, when applied to data with different CR. For every variable there was a polynomial degree for which the daily data trends were better fit by the interpolation. While indoor air temperature data were more accurately described by cubic correlations, relative humidity and  $CO_2$  concentration data had, respectively, more linear and quadratic trends. However, all autoencoders performed by a large margin better than baseline approaches for all variables. In particular, the performance of the convolutional configuration outperformed, in average, all the alternative models. In this regard, the RMSE was 37 % lower than cubic interpolation for indoor air temperature, 24 % lower than linear interpolation for relative humidity and 30 % lower than quadratic interpolation for  $CO_2$  concentration. In terms of NRMSE, missing relative humidity data could be reconstructed with higher accuracy, when compared to other variables. On that place, the worst behavior was obtained with  $CO_2$  data. In particular, the NRMSE of the convolutional configuration in case of  $RH$  data was 75 % lower than  $T$  and 90 % lower than  $CO_2$ . These results were consistent with the SAT trend, being higher for  $RH$  and lower for  $CO_2$  (Table 3).

Figure 9 shows exemplary indoor environment data reconstruction over one random day from the test sets. All presented data were corrupted with a masking noise of 0.5. The presented data confirmed once again the results presented in Table 4, namely, that the proposed denoising autoencoder architectures were suitable for filling the missing indoor environment data sequences.

Table 4: Performance of denoising autoencoder neural networks and polynomial interpolations for reconstructing sub-daily indoor environment data gaps. "CONV", "FEED" and "LSTM" stand for convolutional, feed-forward and LSTM denoising autoencoder. "LIN", "QUAD" and "CUB" stand for linear, quadratic and cubic interpolation.

	CR [-]	$T$ [C]			$RH$ [%]			$CO_2$ [ppm]		
		CONV	FEED	LSTM	CONV	FEED	LSTM	CONV	FEED	LSTM
RMSE	0.10	0.22	0.32	0.33	0.73	1.14	1.05	49.10	64.58	64.88
	0.20	0.31	0.36	0.47	0.90	1.23	1.47	61.16	69.41	82.51
	0.30	0.36	0.42	0.53	1.08	1.35	1.78	69.11	75.04	89.00
	0.40	0.41	0.47	0.59	1.23	1.45	2.11	78.25	81.46	101.64
	0.50	0.46	0.51	0.62	1.36	1.59	2.33	84.12	89.98	107.85
	0.60	0.50	0.53	0.64	1.48	1.66	2.54	91.59	95.38	110.28
	0.70	0.51	0.52	0.63	1.54	1.66	2.72	91.43	94.86	106.16
	0.80	0.50	0.51	0.61	1.66	1.74	2.80	91.26	94.32	102.18
	0.90	0.50	0.49	0.60	1.73	1.78	3.00	89.63	90.52	96.75
Average		0.42	0.46	0.56	1.30	1.51	2.20	78.41	83.95	95.69
NRMSE [-]	0.10	0.15	0.21	0.22	0.04	0.07	0.06	0.43	0.56	0.56
	0.20	0.21	0.24	0.31	0.05	0.07	0.08	0.53	0.61	0.72
	0.30	0.24	0.28	0.35	0.06	0.08	0.10	0.60	0.66	0.78
	0.40	0.27	0.31	0.39	0.07	0.08	0.12	0.68	0.71	0.88
	0.50	0.31	0.34	0.41	0.08	0.09	0.13	0.73	0.79	0.94
	0.60	0.33	0.35	0.42	0.09	0.10	0.14	0.80	0.83	0.96
	0.70	0.34	0.35	0.42	0.09	0.10	0.15	0.80	0.83	0.92
	0.80	0.33	0.34	0.41	0.10	0.10	0.16	0.80	0.82	0.89
	0.90	0.33	0.33	0.40	0.10	0.10	0.17	0.78	0.79	0.84
Average		0.28	0.31	0.37	0.07	0.09	0.12	0.68	0.73	0.83
		LIN	QUAD	CUB	LIN	QUAD	CUB	LIN	QUAD	CUB
RMSE	0.10	0.58	0.52	0.39	1.31	1.10	0.94	94.89	79.97	72.00
	0.20	0.67	0.64	0.49	1.48	1.28	1.13	106.67	92.86	85.32
	0.30	0.73	0.73	0.57	1.59	1.45	1.29	114.41	102.74	96.76
	0.40	0.78	0.82	0.66	1.70	1.59	1.49	118.96	113.61	113.68
	0.50	0.80	0.91	0.74	1.77	1.76	1.69	121.94	122.14	125.89
	0.60	0.79	0.95	0.82	1.82	1.89	1.89	121.25	124.12	148.58
	0.70	0.77	0.95	0.82	1.86	2.01	2.03	120.32	122.30	138.57
	0.80	0.75	0.92	0.70	1.88	2.21	2.31	117.48	122.40	120.25
	0.90	0.74	0.86	0.77	1.91	3.15	3.24	112.40	126.33	125.01
Average		0.73	0.81	0.66	1.70	1.83	1.78	114.26	111.83	114.01
NRMSE [-]	0.10	0.39	0.34	0.27	0.07	0.06	0.05	0.83	0.69	0.63
	0.20	0.45	0.42	0.33	0.08	0.07	0.06	0.93	0.81	0.74
	0.30	0.49	0.48	0.38	0.09	0.08	0.07	1.00	0.89	0.84
	0.40	0.52	0.55	0.44	0.09	0.09	0.08	1.03	0.99	0.99
	0.50	0.53	0.60	0.49	0.10	0.10	0.09	1.06	1.06	1.10
	0.60	0.53	0.63	0.54	0.10	0.11	0.11	1.05	1.08	1.29
	0.70	0.51	0.63	0.54	0.10	0.11	0.11	1.05	1.07	1.21
	0.80	0.51	0.61	0.46	0.11	0.12	0.13	1.02	1.07	1.05
	0.90	0.49	0.57	0.51	0.11	0.18	0.18	0.98	1.10	1.09
Average		0.49	0.54	0.44	0.09	0.10	0.10	0.99	0.97	0.99

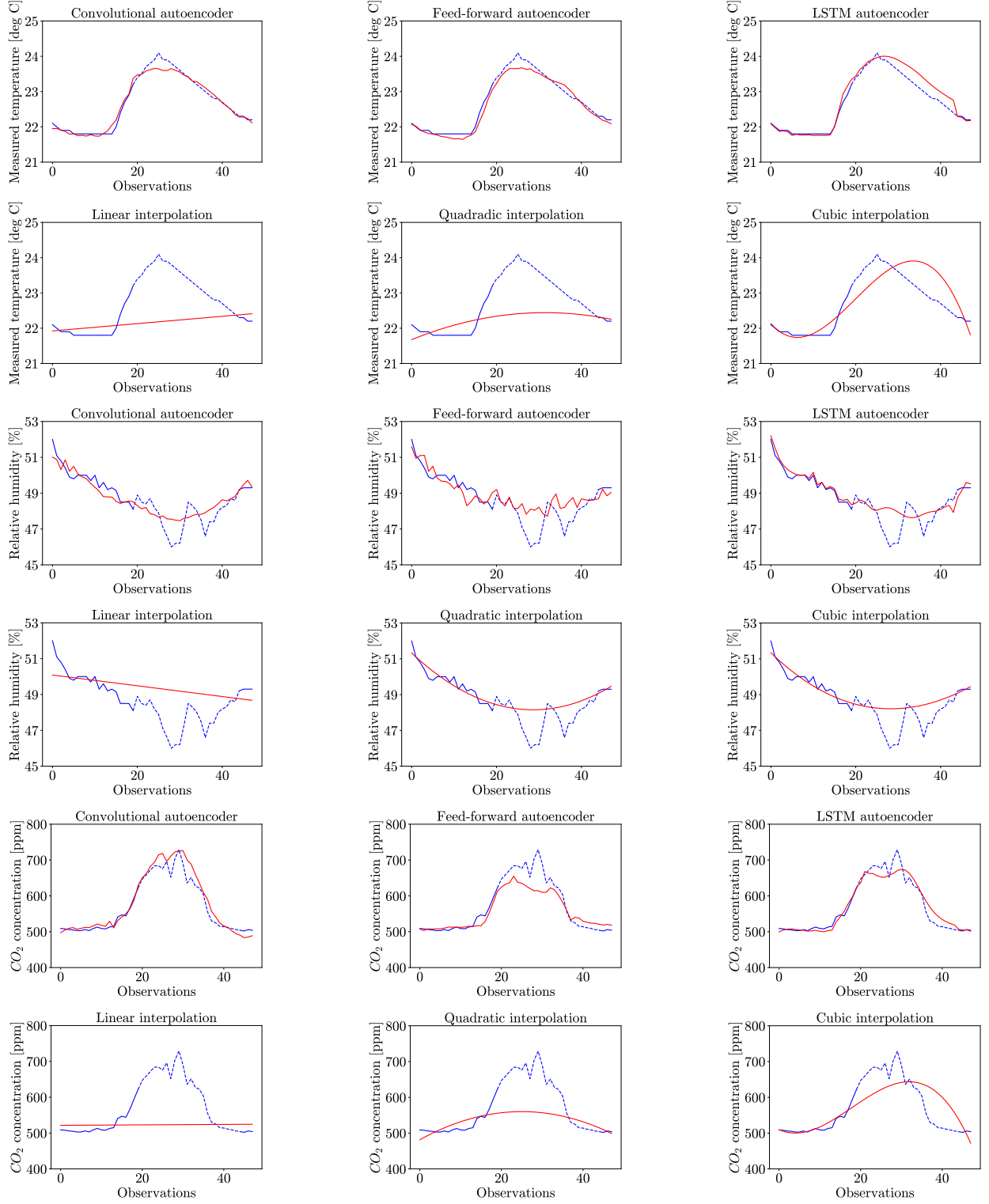


Figure 9: One day-long indoor environment data reconstruction. Blue colored line represents the real data. Hashed blue colored line represents the missing data. Red colored line represents the reconstruction of the whole day with the adopted model. Observations were sampled to 30 minutes steps.

#### 4.4. Data forecasting performance evaluation

As presented in earlier sections, the proposed autoencoder neural networks were implemented to reconstruct sub-daily indoor environment data gaps, since building data sets often contain missing values that could hinder further energy analysis. Nonetheless, the same models could be also used for short-term indoor environment data forecasting.

Table 5 summarizes the performance of the implemented autoencoders for different predictive horizons. In summary, all the models performed similarly well. However, there was a clear improvement, with respect to the data reconstruction case, in the LSTM configuration. In particular, the RMSE of the LSTM model was 14 % lower for indoor air temperature and 20 % lower for  $CO_2$  concentration. In terms of NRMSE, even in this case, the proposed autoencoder neural networks could forecast relative humidity data better than other variables. In particular, the NRMSE of the LSTM configuration in case of  $RH$  data was 59 % lower than  $T$  and 80 % lower than  $CO_2$  data (Table 5).

Table 5: Performance of denoising autoencoder neural networks for forecasting indoor environment data. "CONV", "FEED" and "LSTM" stand for convolutional, feed-forward and LSTM denoising autoencoder. PH is the predictive horizon.

	PH [h]	$T$ [C]			$RH$ [%]			$CO_2$ [ppm]		
		CONV	FEED	LSTM	CONV	FEED	LSTM	CONV	FEED	LSTM
RMSE	2.50	0.19	0.18	0.17	0.89	0.97	0.89	25.62	23.86	25.34
	5.00	0.31	0.30	0.29	1.47	1.44	1.37	43.00	42.38	39.33
	7.00	0.42	0.41	0.40	1.72	1.83	1.76	55.62	55.29	56.11
	9.50	0.50	0.48	0.46	2.15	2.21	2.18	72.37	72.84	74.21
	12.00	0.55	0.52	0.52	2.47	2.45	2.41	81.27	82.55	82.11
	14.50	0.62	0.60	0.59	2.88	2.85	2.67	102.71	102.40	104.51
	17.00	0.73	0.66	0.66	2.84	2.88	2.81	108.13	107.22	107.79
	19.00	0.74	0.64	0.63	2.93	2.95	2.84	102.40	101.58	102.02
	21.50	0.75	0.60	0.60	3.01	3.01	3.18	96.89	96.14	96.88
Average		0.53	0.49	0.48	2.26	2.29	2.23	76.45	76.03	76.48
NRMSE [-]	2.50	0.13	0.12	0.11	0.05	0.05	0.05	0.22	0.21	0.22
	5.00	0.20	0.20	0.19	0.08	0.08	0.08	0.37	0.37	0.34
	7.00	0.28	0.27	0.27	0.10	0.10	0.10	0.48	0.48	0.49
	9.50	0.33	0.32	0.31	0.12	0.12	0.12	0.63	0.63	0.65
	12.00	0.36	0.35	0.35	0.14	0.14	0.14	0.71	0.72	0.71
	14.50	0.41	0.40	0.40	0.16	0.16	0.15	0.89	0.89	0.91
	17.00	0.48	0.44	0.44	0.16	0.17	0.16	0.94	0.93	0.94
	19.00	0.49	0.42	0.42	0.17	0.17	0.16	0.89	0.88	0.89
	21.50	0.50	0.40	0.40	0.17	0.17	0.18	0.84	0.84	0.84
Average		0.35	0.32	0.32	0.13	0.13	0.13	0.66	0.66	0.67

Figure 10 shows exemplary indoor environment data reconstruction over one random day from the test sets. All presented data were corrupted with a masking noise of 0.5 at the end of each time step (predictive horizon of 12 h). The presented data confirmed once again the results presented in Table 5, namely, that the proposed denoising autoencoder architectures were also suitable for the short-term indoor environment data forecasting.

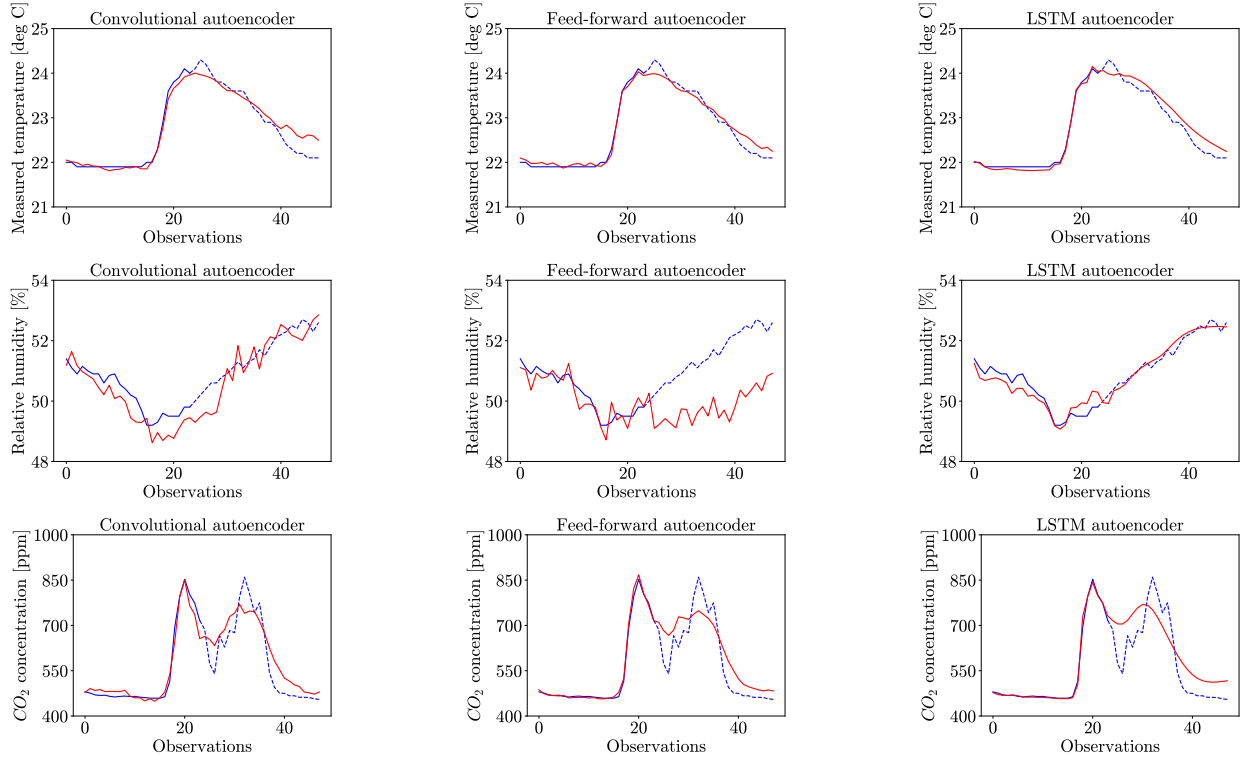


Figure 10: One day-long indoor environment data forecasting. Blue colored line represents the real data. Hashed blue colored line represents the missing data. Red colored line represents the reconstruction of the whole day with the adopted model. Observations were sampled to 30 minutes steps.

## 5. Discussion and future work

The aim of this study was to reconstruct sub-daily indoor environment data time-series since short-term missing data are often present in building data sets and they could hinder further energy analysis. Considering that building energy models usually require inputs at an hourly resolution [8], feeding the models with minute-wise time-series would have resulted in a significant increase of computational costs. Consequently, it was opted for a 30 minutes frequency to conduct further models' development. An important contribution of this paper is the analysis of autoencoder neural networks' performance on different types of environmental time-series, measured over multiple years in a whole commercial building. Accordingly, this fills an important research gap present in the related literature, since existing studies either focused on reconstructing a single type of data stream or they were limited by the size of the available training set.

As presented in Section 3, data were split in three sets before normalization. Model training was performed using a training set, the optimal model configuration was chosen based on performance on the validation set and the data reconstruction accuracy was evaluated using the test set. Approximately 94,085 full days of observations were available, which makes this study – as far as the authors know – the largest of its kind for indoor environment data time-series reconstruction purposes. In order to guarantee a significant generalization of the models, it was decided to take an extensive test set. Accordingly, approximately 2.7 million data points were used for models' evaluation. Improved performance of the final models could be achieved by introducing the dimension of each data set as an additional hyperparameter. However, this choice would have led to additional computational costs and, therefore, it was not pursued.

In total, 1,890 hyperparameter combinations were explored by applying a grid search. Simulations were performed using compute sources granted at RWTH Aachen University. In particular, approximately 7,000 core hours were exploited under project rwth0622.



This work provided important insights regarding the occurrence of the neural networks saturation for analytics related to building's performance. The consequence of model saturation was that the weights were not updated due to the vanishing gradient problem (Section 4.2), which led always to identical predicted values. This problem was observed in case of the convolutional and feed-forward autoencoders, while it was not detected in case of the LSTM autoencoders. The suitable approach to tackle the model saturation was explored in the existing literature on computer vision and general machine learning. Even though all the computed saturation metrics were well above the defined saturation limit (0.1), the SAT decreased with the corruption rate for both indoor air temperature and  $CO_2$  concentration and remained almost unchanged for relative humidity. This was inconsistent with the increasing RMSE trend of the latter variable (Table 4). It can be concluded that the above saturation metric could not be used as an additional performance measure, since it was dependent also on the sequence-variability of the original data. In particular, the worst saturation performance on  $CO_2$  data could be explained with the presence of more extreme values and frequent peaks. This could explain the reason why LSTM neural networks suffered saturation issues in the paper proposed by Markovic et al. [37]. In this earlier study, an LSTM-based model was applied to plug-in loads data and saturation occurred in more than 70 % of the trained configurations. This could be caused by the larger data imbalance of the plug-in loads and the extreme values. Namely, similarly to plug-in loads, the time-series of  $CO_2$  concentration consist of frequent peaks and extreme values, which showed to be a particular complexity to be considered when using the LSTM for building's energy analysis.

The data reconstruction analysis, applied to the non corrupted data, revealed that the proposed autoencoder neural networks, especially the LSTM configuration, could accurately evaluate the indoor environment patterns. Accordingly, this represents a significant practical potential for the inclusion of these methods in the real time building control. This could be used for anomaly detection purposes, by identifying data sequences with atypical behavior (e.g. noisy data, sensors' malfunctioning) (Figure 8). On the other hand, the performance of the convolutional configuration spiked out when a certain masking noise was applied to the test sequences. It can be, therefore, stated that the spatial correlations of input data were more important than the temporal ones, when a gap-filling method was investigated. Additionally, the NRMSE analysis established that relative humidity data patterns were, in general, easier to detect by the proposed models. In order to increase the generalization capability of the developed methods, the inclusion of monitoring data collected in multiple buildings with significant differences in thermal mass and design should be further researched.

Some of possible applications of this study are the use of autoencoder neural networks for time-series data forecasting. In this regard, the performance of the proposed models are really promising and should be considered as part of future expansions of this work. Accordingly, the proposed models could forecast the indoor air temperature data even better than calibrated Modelica-based building performance simulation tools applied in other studies [60]. The temporal correlations of input data gained significant importance with respect to the reconstruction case, placing the LSTM configuration on a slightly better performance level than the convolutional one. Based on the previous considerations, a denoising autoencoder which relies, at the same time, on LSTM and convolutional units could further increase the predictive accuracy of the model. Future work should also evaluate the implemented autoencoders for forecasting energy and environmental data time-series over longer time horizons. The ability of these methods to capture indoor environment data patterns could be further exploited by modelling the energy-related users actions in an unsupervised manner.

Additionally, the proposed models could be used as back-up option in case of sensor failure in the real time building control [7, 13]. In that case, missing data insertion could be effective over the current day of observation.

One of the possible limitations of this study is a direct consequence of the training process. The proposed autoencoders were, indeed, implemented to capture information related to the daily trends of the observed variables. Accordingly, day-ahead data sequences cannot be reconstructed with the current training scheme. Conclusively, the applicability of the proposed models for reconstructing indoor environment data in other buildings has not yet been tested.

## 6. Conclusion

The aim of this paper was to develop an approach for reconstructing indoor environment data time-series. For that purpose, three autoencoder neural networks models were implemented and polynomial interpolation methods were

evaluated for baseline comparison. The evaluation of model performance was conducted using indoor air temperature, relative humidity and  $CO_2$  concentration data. The key findings could be summarized as follows:

- Autoencoder neural networks outperformed polynomial interpolation methods for filling environmental data gaps.
- The convolutional configuration worked better than other models. In this regard, temperature, relative humidity and  $CO_2$  data could be reconstructed with average RMSE (from 10 % to 90 % masking noise) respectively of 0.42 C, 1.30 % and 78.41 ppm.
- Autoencoder neural networks could be used for predicting the indoor environment data with high accuracy, over the multi hour time horizon. The proposed models outperformed calibrated building performance simulation with approximately 56 % lower error rate, in terms of indoor air temperature [60].
- The implementation of normalized initial weights, ReLU activation function and batch-normalization for feed-forward and convolutional autoencoders avoided network saturation.
- Network saturation was not an issue for neural networks with LSTM layers, since they could overcome the gradient vanishing problem.

## 7. Acknowledgements

Part of this work was funded by the Deutsche Forschungsgemeinschaft (DFG, German Research Foundation) – TR 892/4-1 – and by the German Federal Ministry of Economics and Energy (BMWi) as per resolution of the German Parliament under the funding code 03EN1002A. Simulations were performed with computing resources granted by RWTH Aachen University under project rwth0622. We thank the EBC Institute, E.ON ERC at RWTH Aachen University for providing the monitoring data. This paper benefited greatly from discussions with members of IEA EBC Annex 79.

## References

- [1] Directive (EU) 2018/844 of the European Parliament and of the Council of 30 May 2018 amending Directive 2010/31/EU on the energy performance of buildings and Directive 2012/27/EU on energy efficiency. Official Journal of the European Union 61 (2018) 75-76.  
<http://data.europa.eu/eli/dir/2018/844/oj>.
- [2] N. Fumo. A review on the basics of building energy estimation. *Renewable & Sustainable Energy Reviews* 31 (2014) 53-60.  
<https://doi.org/10.1016/j.rser.2013.11.040>.
- [3] I. Khan, A. Capozzoli, S.P. Corngati, T. Cerquitelli. Fault Detection Analysis of Building Energy Consumption Using Data Mining Techniques. *Energy Procedia* 42 (2013) 557-566.  
<https://doi.org/10.1016/j.egypro.2013.11.057>.
- [4] 2009 ASHRAE Handbook-Fundamentals. ASHRAE Inc 404 (2009) 636-8400.  
<http://www.ashrae.org>.
- [5] R. Markovic, E. Grntal, D. Wilki, J. Frisch, C. van Treeck. Window opening model using deep learning methods. *Building and Environment* 145 (2018) 319-329.  
<https://doi.org/10.1016/j.buildenv.2018.09.024>.
- [6] F. Causone, S. Carlucci, M. Ferrando, A. Marchenko, S. Erba. A data-driven procedure to model occupancy and occupant-related electric load profiles in residential buildings for energy simulation. *Energy and Buildings* 202 (2019) 109342.  
<https://doi.org/10.1016/j.enbuild.2019.109342>.
- [7] R. Markovic. Generic occupant behavior modeling for commercial buildings. Doctoral Thesis. RWTH Aachen University. (2020).
- [8] A. Chong, K.P. Lam, W. Xu, O.T. Karaguzel, Y. Mo. Imputation of missing values in building sensor data. ASHRAE and IBPSA-USA SimBuild 2016 Building Performance Modeling Conference. Salt Lake City, UT (2016).  
<http://www.ibpsa-usa.org/index.php/ibpsa/article/view/386/372>.
- [9] L.M. Candanedo, V. Feldheim, D. Deramaix. Reconstruction of the indoor temperature dataset of a house using data driven models for performance evaluation. *Building and Environment* 138 (2018) 250-261.  
<https://doi.org/10.1016/j.buildenv.2018.04.035>.
- [10] J. Ma, J.C.P. Cheng, F. Jiang, W. Chen, M. Wang, C. Zhai. A bi-directional missing data imputation scheme based on LSTM and transfer. *Energy and Buildings* 216 (2020) 109941.  
<https://doi.org/10.1016/j.enbuild.2020.109941>.
- [11] J.S. Haberl, T.A. Reddy, D.E. Claridge, W.D. Turner, D.L. O'Neal, W.M. Heffington. Measuring energy-saving retrofits: experiences from the Texas LoanSTAR Program. United States (1996).  
<https://doi.org/10.2172/219427>.
- [12] A.J. Zapata-Sierra, A. Cama-Pinto, F.G. Montoya, A. Alcayde, F. Manzano-Agugliaro. Wind missing data arrangement using wavelet based techniques for getting maximum likelihood. *Energy Conversion and Management* 185 (2019) 552-561.  
<https://doi.org/10.1016/j.enconman.2019.01.109>.
- [13] J. Loy-Benitez, S. Heo, C. Yoo. Imputing missing indoor air quality data via variational convolutional autoencoders: Implications for ventilation management of subway metro systems. *Building and Environment* 182 (2020) 107135.  
<https://doi.org/10.1016/j.buildenv.2020.107135>.
- [14] C. Fan, F. Xiao, Y. Zhao, J. Wang. Analytical investigation of autoencoder-based methods for unsupervised anomaly detection in building energy data. *Applied Energy* 211 (2018) 1123-1135.  
<https://doi.org/10.1016/j.apenergy.2017.12.005>.
- [15] Y. Liu, Z. Pang, M. Karlsson, S. Gong. Anomaly detection based on machine learning in IoT-based vertical plant wall for indoor climate control. *Building and Environment* 183 (2020) 107212.  
<https://doi.org/10.1016/j.buildenv.2020.107212>.
- [16] D.B. Araya, K. Grolinger, H.F. ElYamany, M.A.M. Capretz, G. Bitsuamlak. Collective contextual anomaly detection framework for smart buildings. 2016 International Joint Conference on Neural Networks, IJCNN, (2016) 511518.  
<https://doi.org/10.1109/IJCNN.2016.7727242>.
- [17] I. Goodfellow, Y. Bengio, A. Courville. *Deep Learning*. MIT Press (2016).  
<http://www.deeplearningbook.org>.
- [18] D.H. Tran, D.L. Luong, J.S. Chou. Nature-inspired metaheuristic ensemble model for forecasting energy consumption in residential buildings. *Energy* 191 (2020) 116552.  
<https://doi.org/10.1016/j.energy.2019.116552>.
- [19] M. Ibeigi, M. Ghomeishi, A. Dehghanbanadaki. Prediction and optimization of energy consumption in an office building using artificial neural network and a genetic algorithm. *Sustainable Cities and Society* 61 (2020) 102325.  
<https://doi.org/10.1016/j.scs.2020.102325>.
- [20] X.J. Luo, L.O. Oyedele, A.O. Ajayi, O.O. Akinade, H.A. Owolabi, A. Ahmed. Feature extraction and genetic algorithm enhanced adaptive deep neural network for energy consumption prediction in buildings. *Renewable and Sustainable Energy Reviews* 131 (2020) 109980.  
<https://doi.org/10.1016/j.rser.2020.109980>.
- [21] N. Somu, G.R. M R, K. Ramamritham. A hybrid model for building energy consumption forecasting using long short term memory networks. *Applied Energy* 261 (2020) 114131.  
<https://doi.org/10.1016/j.apenergy.2019.114131>.
- [22] J.R.S. Iruela, L.G.B. Ruiz, M.C. Pegalajar, M.I. Capel. A parallel solution with GPU technology to predict energy consumption in spatially distributed buildings using evolutionary optimization and artificial neural networks. *Energy Conversion and Management* 207 (2020) 112535.  
<https://doi.org/10.1016/j.enconman.2020.112535>.
- [23] F. Qian, W. Gao, Y. Yang, D. Yu. Potential analysis of the transfer learning model in short and medium-term forecasting of building HVAC energy consumption. *Energy* 193 (2020) 116724.

- <https://doi.org/10.1016/j.energy.2019.11672>.
- [24] Y. Gao, Y. Ruan, C. Fang, S. Yin. Deep learning and transfer learning models of energy consumption forecasting for buildings with poor information data. *Energy and Buildings* 223 (2020) 110156.  
<https://doi.org/10.1016/j.enbuild.2020.110156>.
  - [25] G. Zhang, C. Tian, C. Li, J.J. Zhang, W. Zuo. Accurate forecasting of building energy consumption via a novel ensembled deep learning method considering the cyclic feature. *Energy* 201 (2020) 117531.  
<https://doi.org/10.1016/j.energy.2020.117531>.
  - [26] D.K. Bui, T.N. Nguyen, T.D. Ngo, H. Nguyen-Xuan. An artificial neural network (ANN) expert system enhanced with the electromagnetism-based firefly algorithm (EFA) for predicting the energy consumption in buildings. *Energy* 190 (2020) 116370.  
<https://doi.org/10.1016/j.energy.2019.116370>.
  - [27] Y. Tian, J. Yu, A. Zhao. Predictive model of energy consumption for office building by using improved GWO-BP. *Energy Reports* 6 (2020) 620-627.  
<https://doi.org/10.1016/j.egyr.2020.03.003>.
  - [28] C. Zhou, Z. Fang, X. Xu, X. Zhang, Y. Ding, X. Jiang, Y. Ji. Using long short-term memory networks to predict energy consumption of air-conditioning systems. *Sustainable Cities and Society* 55 (2020) 102000.  
<https://doi.org/10.1016/j.scs.2019.102000>.
  - [29] Y. Meng, T. Li, G. Liu, S. Xu, T. Ji. Real-time dynamic estimation of occupancy load and an air-conditioning predictive control method based on image information fusion. *Building and Environment* 173 (2020) 106741.  
<https://doi.org/10.1016/j.buildenv.2020.106741>.
  - [30] K. Yan, A. Chong, Y. Mo. Generative adversarial network for fault detection diagnosis of chillers. *Building and Environment* 172 (2020) 106698.  
<https://doi.org/10.1016/j.buildenv.2020.106698>.
  - [31] K. Yan, J. Huang, W. Shen, Z. Ji. Unsupervised learning for fault detection and diagnosis of air handling units. *Energy and Buildings* 210 (2020) 109689.  
<https://doi.org/10.1016/j.enbuild.2019.109689>.
  - [32] C. Hengda, C. Huanxin, L. Zhengfei, C. Xiangdong. Ensemble 1-D CNN diagnosis model for VRF system refrigerant charge faults under heating condition. *Energy and Buildings* 224 (2020) 110256.  
<https://doi.org/10.1016/j.enbuild.2020.110256>.
  - [33] Z. Zhou, G. Li, J. Wang, H. Chen, H. Zhong, Z. Cao. A comparison study of basic data-driven fault diagnosis methods for variable refrigerant flow system. *Energy and Buildings* 224 (2020) 110232.  
<https://doi.org/10.1016/j.enbuild.2020.110232>.
  - [34] M. Han, R. May, X. Zhang, X. Wang, S. Pan, D. Yan, Y. Jin. A novel reinforcement learning method for improving occupant comfort via window opening and closing. *Sustainable Cities and Society* 61 (2020) 102247.  
<https://doi.org/10.1016/j.scs.2020.102247>.
  - [35] A. Das, M.K. Annaqeeb, E. Azar, V. Novakovic, M.B. Kjrgaard. Occupant-centric miscellaneous electric loads prediction in buildings using state-of-the-art deep learning methods. *Applied Energy* 269 (2020) 115135.  
<https://doi.org/10.1016/j.apenergy.2020.115135>.
  - [36] R. Markovic, J. Frisch, C. Treeck. Learning short-term past as predictor of window opening-related human behavior in commercial buildings. *Energy and Buildings* 185 (2019) 1-11.  
<https://doi.org/10.1016/j.enbuild.2018.12.012>.
  - [37] Under review: R. Markovic, M.K. Annaqeeb, J. Frisch, C. Treeck, E. Azar. Day-ahead prediction of plug-in loads using a long short-term memory neural network. *Energy and Buildings* (2019).
  - [38] B.K. Beaulieu-Jones, J.H. Moore. Missing data imputation in the electronic health record using deeply learned autoencoders. *Pacific Symposium on Biocomputing* 22 (2017) 207-218.  
[https://doi.org/10.1142/9789813207813\\_0021](https://doi.org/10.1142/9789813207813_0021).
  - [39] G. Bode, T. Schreiber, M. Baranski, D. Miller. A time series clustering approach for Building Automation and Control Systems. *Applied Energy* 238 (2019) 1337-1345.  
<https://doi.org/10.1016/j.apenergy.2019.01.196>.
  - [40] P. Vincent, H. Larochelle, I. Lajoie, Y. Bengio, P.A. Manzagol. Stacked Denoising Autoencoders: Learning useful representations in a Deep Network with a Local Denoising Criterion. *Journal of Machine Learning Research* 11(12) (2010) 3379-3382.  
<http://portal.acm.org/citation.cfm?id=1953039>.
  - [41] J.P. Ffiterer, A. Constantin. Energy concept for the E.ON ERC main building. E.ON Energy Research Center 4 (2014).  
<https://publications.rwth-aachen.de/record/443118>.
  - [42] J.P. Ffiterer, A. Constantin, M. Schmidt, R. Streblow, D. Miller, E. Kosmatopoulos. A multifunctional demonstration bench for advanced control research in buildings Monitoring, control, and interface system. *IECON 2013 - 39th Annual Conference of the IEEE Industrial Electronics Society, Vienna* (2013) 5696-5701.  
<http://dx.doi.org/10.1109/IECON.2013.6700068>.
  - [43] G. Bode, J. Ffiterer, D. Miller. Ein Demonstrator fr innovative Technologien und Konzepte. TGA-Kongress 2016 Berlin (2016).  
<http://publications.rwth-aachen.de/record/660706/files/Vortragsfolien.pdf>.
  - [44] M. Baranski, A. Kmpel, T.P. Schild, M.H. Schraven, F. Stinner, T.P.B. Storek, D. Miller, J. Ffiterer. Ein flexibles lebendes Labor fr die Entwicklung und Erprobung von Cloud-basierten Regelungsalgorithmen fr die Gebudeautomation. *Deutscher Klte- und Klimatechnischer Verein (DKV) e.V.: Tagung 2018, 2018-11-21 - 2018-11-23, Aachen* (2018).  
<http://publications.rwth-aachen.de/record/750585>.
  - [45] The HDF Group. Hierarchical Data Format, version 5, 1997-2020.  
<http://www.hdfgroup.org/HDF5/>.

- [46] Python Core Team (2015). Pickle Python object serialization. Python Software Foundation.  
<https://docs.python.org/3/library/pickle.html>.
- [47] K. Sang, K. Jong. Statistical data preparation: Management of missing values and outliers. Korean Journal of Anesthesiology 70(4) (2017) 407-411.  
<https://doi.org/10.4097/kjae.2017.70.4.407>.
- [48] M. Ferrando, A. Marchenko, S. Erba, F. Causone, S. Carlucci. Pattern Recognition And Classification For Electrical Energy Use In Residential Buildings. Building Simulation 2019, Rome (2019).  
<https://doi.org/10.26868/25222708.2019.210750>.
- [49] M. Rtz, A.P. Javadi, M. Baranski, K. Finkbeiner, D. Mller. Automated data-driven modeling of building energy systems via machine learning algorithms. Energy and Buildings 202 (2019) 109384.  
<https://doi.org/10.1016/j.enbuild.2019.109384>.
- [50] T. Jayalakshmi, A. Santhakumaran. Statistical normalization and back propagation for classification. International Journal of Computer Theory & Engineering 3(1) (2011) 1793-8201.  
<http://www.ijcte.org/papers/288-L052.pdf>.
- [51] M. Abadi, A. Agarwal, P. Barham, E. Brevdo, Z. Chen, C. Citro, G. S. Corrado, A. Davis, J. Dean, M. Devin, S. Ghemawat, I. Goodfellow, A. Harp, G. Irving, M. Isard, R. Jozefowicz, Y. Jia, L. Kaiser, M. Kudlur, J. Levenberg, D. Man, M. Schuster, R. Monga, S. Moore, D. Murray, C. Olah, J. Shlens, B. Steiner, I. Sutskever, K. Talwar, P. Tucker, V. Vanhoucke, V. Vasudevan, F. Vigas, O. Vinyals, P. Warden, M. Wattenberg, M. Wicke, Y. Yu, X. Zheng. TensorFlow: Large-Scale Machine Learning on Heterogeneous Distributed Systems. CoRR (2016).  
<https://arxiv.org/abs/1603.04467v2>.
- [52] F. Chollet. Keras. (2015).  
<https://keras.io>.
- [53] S. Ioffe, C. Szegedy. Batch normalization: accelerating deep network training by reducing internal covariate shift. CoRR (2015).  
<https://arxiv.org/abs/1502.03167v3>.
- [54] I. Sutskever, J. Martens, G. Dahl, G. Hinton. On the importance of initialization and momentum in deep learning. Proceedings of the 30th international conference on machine learning. 28(3) (2013) 11391147.  
<http://proceedings.mlr.press/v28/sutskever13.html>.
- [55] K. Diederik, J. Ba. Adam: A method for stochastic optimization. (2014).  
<https://arxiv.org/abs/1412.6980v9>.
- [56] J. Bergstra, Y. Bengio. Random Search for Hyper-Parameter Optimization. Journal of Machine Learning Research 13 (2012) 281-305.  
<https://dl.acm.org/doi/10.5555/2188385.2188395>.
- [57] X. Glorot, Y. Bengio. Understanding the difficulty of training deep feedforward neural networks. Proceedings of Machine Learning Research 9 (2010) 249-256.  
<http://proceedings.mlr.press/v9/glorot10a.html>.
- [58] R. Grosse. Introduction to Neural Networks and Machine Learning. CSC 321 Winter 2018.  
[http://www.cs.toronto.edu/~rgrosse/courses/csc321\\_2018](http://www.cs.toronto.edu/~rgrosse/courses/csc321_2018).
- [59] A.L. Maas, A.Y. Hannun, A.Y. Ng. Rectifier nonlinearities improve neural network acoustic models. Proceedings of the 30th International Conference on Machine Learning 28 (2013).  
[http://robotics.stanford.edu/~amaas/papers/relu\\_hybrid\\_icml2013\\_final.pdf](http://robotics.stanford.edu/~amaas/papers/relu_hybrid_icml2013_final.pdf).
- [60] R. Markovic, E. Grintal, A. Nouri, J. Frisch, C. Treeck. Right on Time -Exploring Suitable Time Discretization for Occupant Behavior Co-Simulation. Building Simulation 2019, Rome (2019).  
<http://doi.org/10.26868/25222708.2019.210166>.
- [61] D.K. Chaturvedi. Soft computing: techniques and its applications in electrical engineering. Springer 103 (2008) 51-85.  
<https://doi.org/10.1007/978-3-540-77481-5>.

# Appendix

This Appendix provides additional information about the adopted data cleaning process.

## A.1. Outliers

Outliers were detected favoring model generalization, rather than accuracy. The aim of this paper was, indeed, to provide a tool to reconstruct indoor environment time-series, independently of the type and quality of data. Ma et al. [10] applied the IQR method for the reconstruction of building electric power data, defining as outlier every value out of the following range:

$$[Q_1 - 1.5 \cdot IQR; Q_3 + 1.5 \cdot IQR], \quad (10)$$

where  $Q_1$  is the first quartile of the dataset,  $Q_3$  is the third quartile,  $IQR$  is the difference between the third and first quartile. Data out of the previous interval were replaced with the nearest IQR limit [10]. However, since the generalization characteristics of ANNs depend on the noise included in the training data [61], the authors decided not to follow this approach at the expenses of an overall reduced accuracy [61]. Accordingly, outliers were detected based on theoretical limits fixed by Markovic et al. [5] in a different study, where a subset of the same data set was analyzed. Therefore, temperature was established between -10 and +40 °C, based on the plausible range for the continental climate in Germany [5]. Relative humidity was set between 0 and 100 % [5], while  $CO_2$  concentration was assumed to be between 0 and 2,500 ppm [5]. Table 6 summarizes descriptive statistics for the data set before and after outliers detection, based on the methods proposed in the literature [5, 10]. The IQR method proposed by Ma et al. [10] seemed to oversimplify the problem, by identifying as outliers a wide range of values (Table 6). It was, therefore, opted for the other approach [5].

Table 6: Descriptive statistics for the data set before (raw data) and after ([5, 10]) outliers detection. Std and L/U IQR stand respectively for standard deviation and lower/upper IQR limit.

	T [C]			RH [%]			CO <sub>2</sub> [ppm]		
	Raw data	[10]	[5]	Raw data	[10]	[5]	Raw data	[10]	[5]
Min	6	19.4	6	0.5	1.45	0.5	0	265	192
Max	2.34E+16	25.8	37.1	2.53E+03	72.25	99.4	1.31E+04	737	2,000
Mean	6.47E+10	22.64	22.63	3.75E+01	37.52	37.5	5.16E+02	509.12	516.3
Median	22.7	22.7	22.7	36.4	36.4	36.4	491	491	491
Std	3.60E+13	1.22	1.4	1.18E+01	11.01	11	1.25E+02	100.27	124.25
L IQR	19.4	19.4	19.4	1.45	1.45	1.45	265	265	265
U IQR	25.8	25.8	25.8	72.25	72.25	72.3	737	737	737
Outliers	/	2.54E+06	358	/	1.71E+03	313	/	4.18E+06	307

## A.2. Missing values

Based on the logging frequency and monitoring duration, it could be expected that around 181 million sets of observations were collected for each variable from 2014 to 2017. Of the latter, only 73 million data points were correctly recorded for  $T$  (59.6 % error rate), while 70 million for both  $RH$  and  $CO_2$  (61.3 % error rate). In order to increase the computational efficiency of the models, frequency was reduced from minute-wise to 30 minutes, leading to approximately 2.3 million data points for each variable. For the missing values handling, a complete case analysis approach was adopted, where only full day of observations with the current resolution were considered. Hence, the number of available monitoring points per variable were reduced to 1.5 million data. Accordingly, from the starting 376,938 daily observations, models were applied only to 94,085 days (75 % error rate). An overview of the missing values handling strategy is presented in Table 7 and in Figure 11.

Table 7: Overview of the preprocessed data set.

	$T$	$RH$	$CO_2$
Frequency [min]	30	30	30
Expected days	125,646	125,646	125,646
Discarded days	94,265	94,294	94,294
Complete days	31,381	31,352	31,352

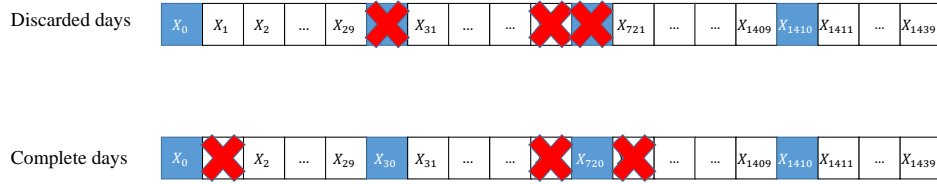


Figure 11: A visual representation of the discarded and complete days. White blocks are minute-wise observations. Blue blocks are observations with 30-minutes frequency resolution.